

DESIGN OF A HIGHLY EFFICIENT TRANSPORT NLF AIRCRAFT WITH A BACKWARD SWEPT WING AND A LONG SINGLE-AISLE FUSELAGE

Thomas Streit¹, Javier Ruberte Bailo², Alexander Büscher³, Arne Seitz⁴

¹DLR, Lilienthalplatz 7, D-38108 Braunschweig, Germany, th.streit@dlr.de
²DLR, Lilienthalplatz 7, D-38108 Braunschweig, Germany, javier.rubertebailo@dlr.de

³Airbus Operations GmbH, Airbus-Allee 1, 28199 Bremen, Germany, alexander.buescher@airbus.com
⁴DLR, Lilienthalplatz 7, D-38108 Braunschweig, Germany, arre.seitz@dlr.de

Abstract

This paper presents results of the numerical aerodynamic design and analysis of a highly efficient passenger aircraft with a backward swept wing (BSW) and a long single-aisle fuselage. Large efficiency is obtained with large aspect ratio wings and using natural laminar flow (NLF) shape designs. Several wing planforms are considered. Design cruise Mach number is increased by considering planforms with increasing wing leading-edge (LE) sweep. For each planform case with a fixed (LE) sweep a detailed NLF wing design was performed for the corresponding cruise design Mach number. With increasing LE sweep, it becomes more difficult to achieve NLF in the inner wing due to crossflow instability. Here, a natural laminar flow (NLF) design was still possible for the largest investigated LE sweep case by using a crossflow attenuated NLF (CATNLF) section design strategy. For the final high swept planform also off-design flow conditions were considered in order to improve the performance for these conditions. A final designed shape was achieved. It provided the flight shape (twist) and jig shape (bending) for a test in the European Transonic Wind Tunnel (ETW). First results of the final wind tunnel geometry are presented.

Keywords: Laminar wing design, transition, NLF, CATNLF, drag reduction

1. Introduction

This work was performed within the German LuFo project ULTIMATE: <u>Ultra high efficient</u> wing and <u>moveables</u> for next generation aircraft. LuFo is the national German Aeronautical Research Program. The LuFo project ULTIMATE is a research collaboration between Airbus, DLR, ETW, Liebherr, Technical University Berlin and the Technical University Hamburg.

Due to growing air traffic, the impact of aviation emissions on climate and the so far limited capacity and costly production of sustainable fuels commercial aviation requires significant changes. One step in the development to more sustainable aviation is the design of more efficient future aircraft. In this work the ULTIMATE NLF BSW wing design study led to a geometry with improved aerodynamic efficiency, which is going to be tested in the ETW. Despite being a conventional transport wing body geometry, in comparison to existing transport aircraft its wing geometry incorporates modifications which pursue the efficiency of this type of aircraft to its potential limits. On one side the high efficiency of the ULTIMATE NLF BSW wing is obtained using large aspect ratio wings. On the other side, drag is reduced further with a detailed NLF shape design.

In recent years there has been an increased interest in NLF technology as a possibility to increase efficiency by reducing the aerodynamic drag. There have been several NLF wing designs, wind tunnel tests and the NLF technology has been demonstrated in the BLADE flight test [1], [2]. Considering medium range aircraft, one of the NLF wing designs, the DLR-FSW (Forward Swept Wing) [3], [4] is particularly promising in reducing aerodynamic drag. Due to the characteristic low

LE sweep of an FSW, no crossflow or attachment line transition occurs in the nose region. Therefore, a design with a laminar boundary layer region is possible which extends from the wing root to wing tip. Nevertheless, an FSW allows a large local sweep at the shock position, this enables a design with small wave drag contribution at cruise Mach numbers similar to current BSW medium range aircraft designed for turbulent boundary layer. Over the years commercial aircraft industry has gained a large experience in the design, manufacturing and operation of aircraft with a BSW. For an FSW this experience of an entire aircraft is partially missing. In contrast to an FSW, a BSW has the maximum local sweep at the LE. Therefore, in previous NLF BSW designs LE sweep was reduced to avoid transition at the section nose. This resulted also in reduced cruise Mach number to assure reasonable wave drag level. DLR designed an NLF BSW [5] within the European integrated technology demonstrator Smart Fixed Wing Aircraft (SFWA). SFWA was part of the Joint Technology Initiative (JTI) Clean Sky. In the following this NLF BSW design will be denoted DLR-JTI BSW design. In addition, for the DLR-JTI BSW design presented in [5], despite reduced LE sweep, the local inner wing Reynolds numbers were so large that with traditional NLF design early transition occurred close to the nose due to crossflow instabilities. Therefore, in order to obtain laminar flow in the inner wing, LFC was required [5]. With the use of crossflow attenuated NLF (CATNLF) design strategy [7]-[9] crossflow transition can be avoided for LE sweep angles for which otherwise boundary layer suction would be required in the nose region. In this work the pursued aim was to obtain a medium range NLF BSW design with a laminar boundary layer which along the entire wing span and a cruise Mach number close to current turbulent medium range aircraft. This has been realized by stepwise increase of design cruise Mach number and LE sweep. Since the BLADE experiment demonstrated the NLF technology successfully, selected starting values for the ULTIMATE study were the cruise design Mach number and LE sweep of the BLADE NLF panel. The final design for the largest design cruise Mach number then was selected as wind tunnel geometry for the ETW test.

The used wing planforms in the design study show high aspect ratios. This leads to a reduction of induced drag. On one side, the large aspect ratio wing facilitates the NLF design, since the chord Reynolds numbers for the inner wing are smaller than the ones of the previously mentioned NLF wing designs. On the other hand, the selected wing planform in combination with the here used long fuselage (which requires a larger 1g C_L value) causes higher aerodynamic loading in comparison to the previously mentioned NLF designs. This led to a more challenging transonic design. Nevertheless, with a careful design approach which considered the cruise design point as well as off design points, a balanced and acceptable wave drag standard was obtained.

The different wings in this study were designed for flight conditions. After the aerodynamic design work presented here, considerable work is still required to obtain a wind tunnel geometry which can be manufactured. The provided aerodynamic design defines the flight shape twist and the jig shape bending. This work is finalized by obtaining the complete jig shape for the wind tunnel model design and manufacturing.

2. Geometries, flow conditions and design requirements

For the design study wing body configurations are considered. A perspective view of the aircraft is shown in Figure 1. The geometry corresponds to a target 1g flight shape regarding twist, whereas regarding bending it has the jig shape. The wing has a bi-trapezoidal planform. CFD computations consider only half of the aircraft geometry. As mentioned above the design study started with a wing with rather low LE sweep (and reduced cruise design Mach number). After demonstrating that for a certain LE sweep an NLF design is possible which has acceptable laminar boundary layer extent in the inner wing, a wing with increased LE sweep (and cruise design Mach number) is considered next. Starting with the LE sweep of the BLADE NLF panel $\phi_{LE} = \phi_{LE_BLADE}$, the wing LE sweep was increased twice in steps of $\Delta \phi_{LE} = 2.5^{\circ}$. Correspondingly, cruise design Mach number was increased from an initial value $M_{\infty}=0.75$ twice in steps of 0.01. For the determination of transition position with the N-factor method, the incompressible free stream critical N-factors are used [10].

Flow conditions for cruise design points and wing LE sweep are given in Table 1

Table 1 Development of wing planform and Mach number during design study

Geometry		M∞	Δφ _{LE} [°]	
Case	Design status		(φιε = φιε_blade+ Δ φ ιε)	
Α	1	0.75	0.0	
В	2-3	0.76	2.5	
С	4-6,7x	0.77	5.0	

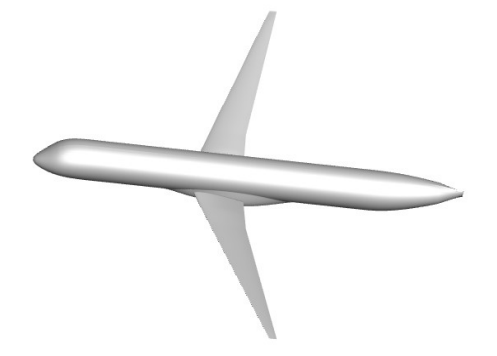


Figure 1 ULTIMATE wing body geometry

The cruise design lift coefficient corresponds to the lift of the 1g condition and is denoted $C_{L_1g}(M_{\odot})$. For some of the different cases, defined by fixed parameters $(M_{\odot},\,\Delta\phi_{\,LE}\,)$, there are different geometries denoted as Design status. Here the Design status represents either an initial geometry or a modified geometry developed by detailed section design or planform adaptations. For case C, Design status 7 defined the final planform, further detailed design modifications are defined as Design status 7x geometries, where x is a variable which stands for an alphabetic ordered letter. In comparison to the NLF DLR-JTI BSW

geometry [5], the design status 7 wing has an aspect ratio which is 49% larger. For delivered geometries RANS solutions are obtained with the DLR CFD solver [6] TAU using fine analysis meshes. For the determination of transition position with the 2-N-factor method, the incompressible free stream critical N-factors are used.

For each case the wing designs have to satisfy following requirements:

<u>Aerodynamic requirements</u>: For the cruise point, the design should not significantly alter the loading distribution of the initial Airbus geometries provided for each case. By satisfying the loading requirement also a prescribed center of lift is achieved.

<u>Thickness requirements</u>: Maximum airfoil thickness of the Airbus initial geometry for each case has to be maintained or slightly increased.

<u>Transition position</u>: For the ULTIMATE BSW wing the laminar region is restricted to the upper side. This is due to the chosen Krüger high-lift system. Current Krüger designs produce surface gaps and steps in retracted position, which make the lower wing surface unsuitable for laminarization.

3. Design, simulation methods and postprocessing Tools

The numerical simulations carried out in the course of this work can be classified into ULTIMATE wing shape design and analysis tasks of the shape designs. The following sections describe the methodology, numerical methods and tools used in each case.

3.1 Design method

For the detailed shape design of the ULTIMATE NLF BSW wing the DLR inverse transonic 3D design method [11] is used. This method allows the design of adapted wing sections using user-specified target pressure distributions. The inverse design method is an integrated module of the DLR FLOWer code [12] for block-structured meshes. The target pressure distributions used are generated with the aim to increase laminar extent and/or reduce shock strength. In the last two decades the DLR inverse code has been the method of choice for the design of laminar wings for transonic flows, more recent design are presented in [3], [5], [13] and [14].

Here, this solver has been chosen as CFD design method since: a) it is a 3D inverse design method, b) the meshes required here are not too complex (allowing structural mesh generation), c) FLOWer

Inverse is a robust, efficient and accurate CFD method, ideal for a large number of design iterations and extensive off-design analysis, d) the design of the ULTIMATE NLF BSW requires CATNLF design for the wings with large LE sweep. With the FLOWer inverse design solver 2.75D (conical sectional design) can be performed for sections of a tapered wing [15]. The computational cost involved is comparable to the computational cost of a 2D or a 2.5D computation. Prior to the 3D inverse wing design, it is useful to perform 2.75D CATNLF design for specific sections of the tapered wing. This is done with the aim to provide geometry initial geometry sections and target pressure distributions for the 3D inverse design of the wing.

3D meshes were generated using a DLR in-house mesh generation software [16], [17] for structured wing-body configurations. A CH-topology is used for the wing-body mesh. Since the main effect of the body on the wing flow is the displacement of the flow, the body is only modelled with an inviscid boundary condition. In this work, analysis of FLOWer CFD solutions for wing body meshes is performed: a) for design: on meshes with 531x321x41 points and with 321x33 (chord direction x span direction) points for the wing surface b) for pre-analysis of designed geometries a finer mesh is generated which is finer in spanwise direction, with 531x321x81 points and with a wing surface with 321x65 points. The fine mesh postprocessing includes stability analysis in order to determine transition positions. In the design (coarse meshes) transition line is fixed and obtained from the fine mesh solution.

3.2 CFD analysis

For the final CFD analysis of the designed geometries fine unstructured meshes are obtained. For this purpose, the wing sections designed with the inverse design process are transferred into a CAD model of the complete aircraft. The CAD model forms the basis for the analysis CFD mesh. CFD solutions were obtained on meshes either provided by Airbus or generated by DLR using the mesh generator SOLAR [18]. With a resolution of about 30·10⁶ mesh points each, these meshes are much finer and more complex than the structured analysis meshes of about 5·10⁶.

For the CFD simulations, DLR's flow solver TAU [6] was used. TAU solves the Reynolds-averaged Navier-Stokes equations (RANS) on a cell vertex, finite volume formulation. For the spatial discretization, a central Jameson scheme with matrix dissipation is applied. Time integration is performed with an implicit backward Euler scheme, using LU-SGS. Turbulence modelling was performed with the kw-Menter-SST 1994 model.

TAU's iterative automatic transition prediction module [19] is employed to evaluate the local laminar/turbulent transition position for a user-defined number of spanwise stations. At each station, pressure distributions and geometrical data are extracted from the current CFD solution and passed to a differential boundary layer solver. Employing the local conical wing assumption, the solver calculates the local boundary layer profiles. The transition location is predicted by means of local linear stability analysis and a 2-N factor transition criterion, calibrated for NLF application. The new transition locations for all considered stations form a transition polyline. The transition polyline is then passed back to the CFD solver to distinguish laminar and turbulent parts of the flow. The process of CFD calculation and transition prediction is repeated iteratively. Convergence is usually reached within six iterations. Details on methods and codes involved in the transition prediction module are given in the following section.

3.3 Methods and tools employed for stability analysis and transition prediction

Despite the emergence of more sophisticated stability analysis methods, linear stability theory (LST) remains the preferred technical tool for stability analysis in computationally intensive design and analysis activities outlined here. Both the design process and the final analysis use the STABTOOL program suite [20], [21] for transition prediction based on local LST.

For the stability analysis of 3D wing boundary layers, the assumption of spanwise locally conical flow conditions is introduced at first. This assumption allows a numerically efficient calculation of the laminar boundary layer profiles per wing section. The boundary layer code *coco* [21] was used to calculate compressible, conical flow boundary layer profiles.

To calculate the growth rates of Tollmien-Schlichting (TS) and cross flow (CF) instability modes the

local linear stability solver *lilo* [20] was employed. To solve the LST eigenvalue problem, a fixed frequency and fixed propagation direction approach is used for TS waves, while a fixed frequency/fixed wavenumber approach is chosen for CF waves. TS mode evaluation is restricted to a propagation direction of Ψ =0°, i.e. along the group velocity direction. For cross flow, only stationary modes (f=0Hz) are considered. Separate N-factors for TS and CF modes are obtained by integrating the respective growth rates along the group velocity direction.

To predict the transition location, a 2-N factor transition criterion is used. The N-factor limit curve used in this work corresponds to the NLF incompressible free stream critical N-factors. In addition, the \overline{Re} criterion is evaluated to assess the likelihood of attachment line transition.

3.4 Postprocessing

Postprocessing of DLR-CFD solutions (TAU and FLOWer) was performed with the DLR wing-body postprocessing software [5]. This tool comprises various different DLR tools which allow in an automatic way to make an analysis of the CFD solution providing pressure distributions, aerodynamic total coefficients, drag breakdown, spanwise distributions of aerodynamic coefficients and corresponding forces and transition related quantities It can be used either for FLOWer or TAU CFD solutions. The postprocessing of Airbus CFD solutions occurs with the ONERA far-field drag analysis software [22], [23]. Both software tools allow a breakdown of drag into physical components, namely viscous, wave and induced drag. A far-field evaluation of drag is more accurate than its near-field counterpart, thus also allowing for a quantification of spurious drag production. In the following drag components will be given related to the total drag of the design status 7g geometry at free stream design point. This value is denoted c_{D 7g f.s}.

.

4. Exploration study of BSW NLF designs with increasing cruise Mach number

The aim of this work is to design an NLF BSW for a larger cruise design Mach number. In this section results are presented for a study of detailed shape designs of NLF BSW with varying LE sweep. The design cruise Mach number is increased accordingly to the wing LE sweep. In this study it is explored up to which cruise design Mach number and corresponding LE sweep an NLF design is still feasible. The study starts with the design cruise Mach number and LE sweep corresponding to the BLADE NLF panel, i.e. for case A. In the study the Mach number was increased in steps of Δ Ma=0.01, the wings LE sweep being increased in steps of $\Delta \phi_{LE}$ =2.5°. After two steps (case B and C), i.e. with total deltas Δ Ma=0.02, $\Delta \phi_{\perp F}$ =5.0°, a detailed wing shape design with laminar boundary was still possible. A robust NLF design for a further step in which Mach number and wing LE sweep were increased was deemed difficult. For the case C, with maximum cruise Mach number and LE sweep, a much more elaborated design is performed, which is described in section 5. CFD solutions for inverse design and CFD pre-analysis solutions are obtained with the simplified structured design meshes. Finally, solutions for final NLF designs of each step are analyzed with TAU CFD solutions on the fine analysis meshes (unstructured meshes). The mesh generation of the structured wing body meshes requires a different input than the corresponding mesh generation of the unstructured meshes. The frequent transfer of wing geometry data for both types of mesh generation was enabled by using specified data format and specific defined procedures.

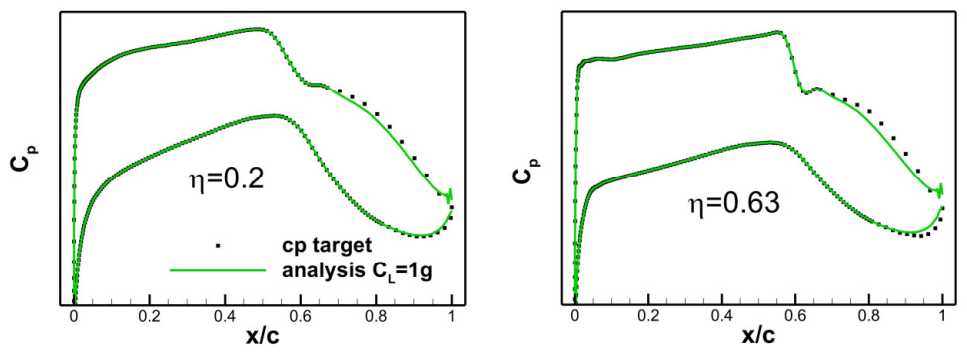


Figure 2: 3D laminar target Cp for case A for sections η =0.20 and η =0.61. Target Cp based on solution with turbulent boundary layer and adapted downstream of shock and in TE region.

4.1 Initial geometry and design target

The initial wing body geometries for these cases were provided by Airbus. Besides the fuselage, the delivered geometries provided the wing planform definition (see Figure 1) and wing airfoil sections at selected span positions. Provided wing sections were designed for laminar flow. For the corresponding design point for these geometries (see Table 1), a RANS solution with turbulent boundary for this initial geometry satisfied the spanwise loading distribution requirement and defined the spanwise thickness distribution. Initial geometries had acceptable low wave drag values. A stability analysis of the CFD solutions of the initial geometries (computed with turbulent boundary layer) showed acceptable upper wing laminar boundary layer extent with transition position occurring near to the shock position except for the inner wing region. The design task was to obtain the corresponding wing for the free transition case. This requires changes of twist and airfoil geometry of the initially provided wings.

For the detailed design the 3D inverse design DLR FLOWer code was used. Design is performed on the simplified structured design meshes. For selected promising design geometries TAU CFD analysis solutions were computed using fine unstructured meshes.

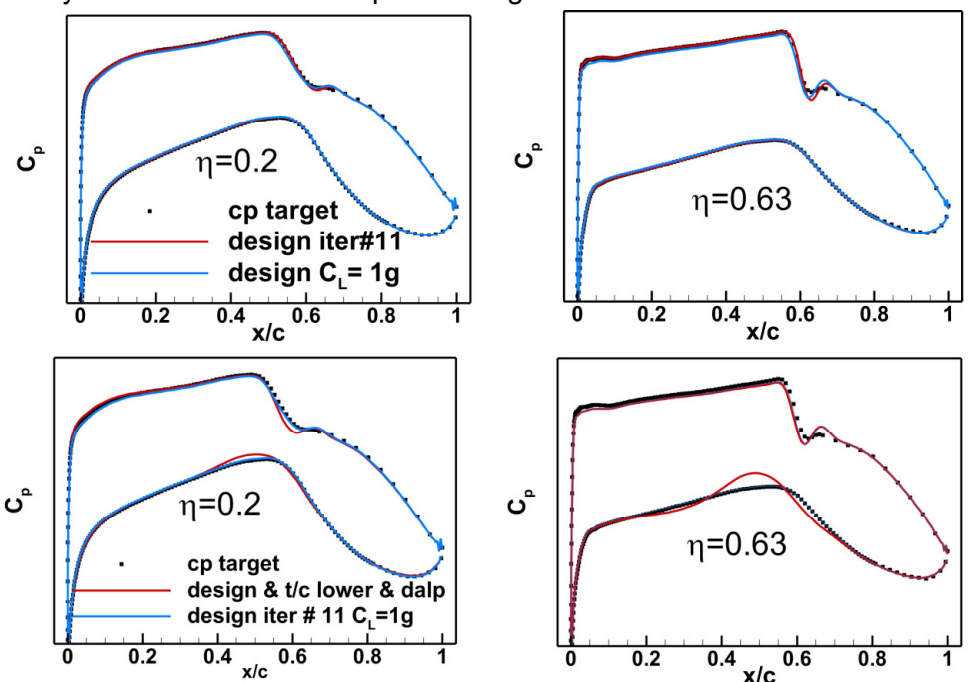


Figure 3 : NLF design for case A, Cp for η =0.20 and η =0.61. Upper row: 3D inverse design using target defined in Figure 2. Lower row: after adaptions to satisfy thickness and circulation requirements.

Since the wing pressure distributions the turbulent boundary solution for the initial geometry provided acceptable laminar extent and low wave drag, this wina pressure distribution was used pressure as distribution target. Note however, that this target pressure distribution additionally requires modification at the upper side in a region upstream of the transition position. This is due to the different turbulent layer upstream of the transition position.

which in the case with transition starts with a smaller boundary layer thickness. The 3D detailed design therefore required a procedure with many steps. This procedure is described next:

- 1. First step: Definition of target pressure distribution. Initial target pressure distribution is obtained from initial geometry RANS solution with turbulent boundary layer. This target pressure distribution has the advantage that it satisfies spanwise the circulation requirement and has acceptable laminar extent. It comprises the whole wing with wing sections defined between span $\eta_{ROOT} \le \eta \le 1.00$. Then, this target pressure distribution is modified on the upper side for the region upstream of the transition position and a region close to the leading-edge on the lower side. Since the transition occurs close to the shock, the target pressure distribution was modified upstream of the shock position. This modification was based on the difference of the pressure distribution obtained between RANS solution of the initial geometry for design lift with turbulent boundary layer and with free stream transition. Figure 2 shows the constructed target pressure distribution.
- 2. Second step: Inverse design with target pressure distribution obtained in step 1. Note that the 3D inverse design will change the twist distribution as well as the airfoil geometry of the wing sections.

Figure 2 shows examples of the initial and modified target pressure distribution modifications for

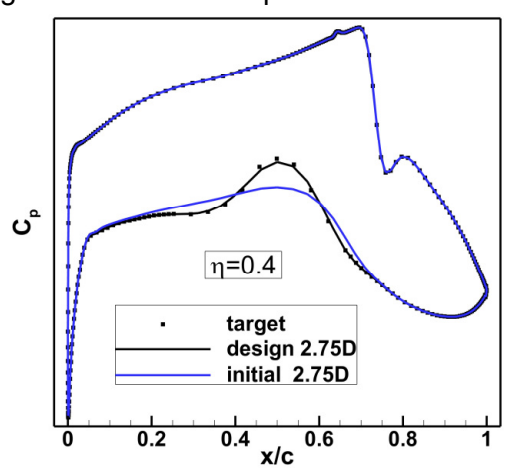


Figure 4 2.75d design for case B, η =0.40: C_p target upper side not modified, lower side modified with the aim to increase thickness.

side preserves the achieved laminar extent and shock properties of the initial geometry. Figure 4 shows the initial, target and resulting designed pressure distribution of the 2.75D design case for the n=0.40 section. The difference in geometry between initial and design on the lower side obtained for η=0.40, is then added with a scaling factor to all defining wing airfoils. The scaling factor is chosen in such a way that the required thickness distribution is obtained. CFD analysis for the third step is performed with refined simplified meshes (65 wing sections).

4. Fourth step: The load distribution for the geometry obtained in the last steps has small differences in comparison to the required load distribution. The load distribution requirement is satisfied by changing the spanwise twist distribution. Figure 3 lower row shows the final pressure distribution after the 3D inverse design (step 2), after thickness modifications (step 3) and twist modification (step 4) for η =0.20 and η =0.61 for the case A cruise design point. CFD analysis for the third step is performed with refined simplified meshes (65 wing sections).

- sections with η =0.20 and η =0.61 for case A. Since the design involves many iterations, the inverse design is obtained with the simplified design mesh (33 wing sections). Results of the design are shown in the upper row of Figure 3. Since design occurs at AoA of the case A start geometry, a solution is also computed for the lift of the case A design point.
- 3. Third step: Due to the thinner laminar boundary layer thickness on the upper side, the designed wing in the second step has airfoils with smaller thickness. With a 2.75D inverse design for the η =0.40 section a modification is performed in which the thickness is regained mainly on the lower side. For that a target pressure distribution is used which for the same local c_i only modifies the pressure distribution on the lower side. On the lower side pressure distribution is modified for 0.1 < x/c < 0.8. Not altering the upper

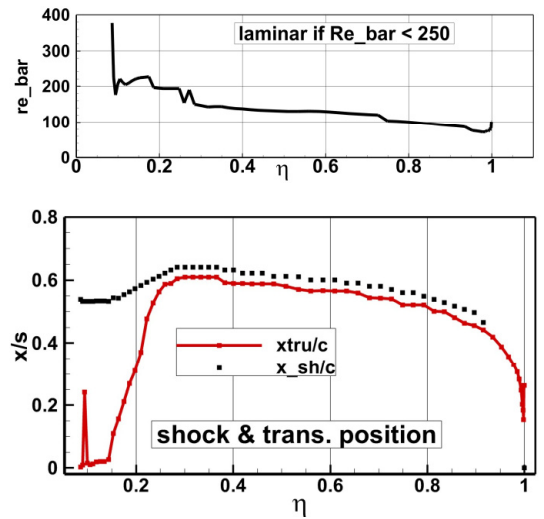


Figure 5: NLF design for case A. Spanwise distributions for attachment line criteria (upper side). Transition and shock position (lower side)

4.2 Detailed NLF shape design for case A, M_∞=0.75, Δφ_{LE}=0.0°

The initial wing body geometry for this case was provided by Airbus and denoted Design status 1. Design was performed at cruise design point (see Table 1). The detailed NLF shape design was obtained using all steps of the previously described design procedure. Therefore, the loading and thickness requirements are satisfied. The inverse design provided an NLF wing which with free transition satisfies the loading distribution requirement. Figure 5, upper plot shows that the transition due to attachment line instability does not occur. Values of \overline{Re} are smaller than 250, which is the contamination threshold. Figure 5, lower plot shows the obtained transition position. The wave drag has an acceptable low value, it is 1.3% of the total drag c_{D 7g f.s}. Transition is close to the shock position, except for an inner wing region where the laminar extent is reduced due to Tollmien-Schlichting transition. Due to the low LE sweep of this case, transition at the nose due to crossflow instability does not occur. Therefore, further improvements of transition position of the inner wing were expected to be possible using traditional NLF design without requiring CATNLF. Thus, no further design was considered for this case and it was decided to continue with increased Mach number i.e. with case B. Using fine unstructured meshes a complete analysis with TAU solutions were obtained for the here designed NLF geometry at cruise point and at off design conditions.

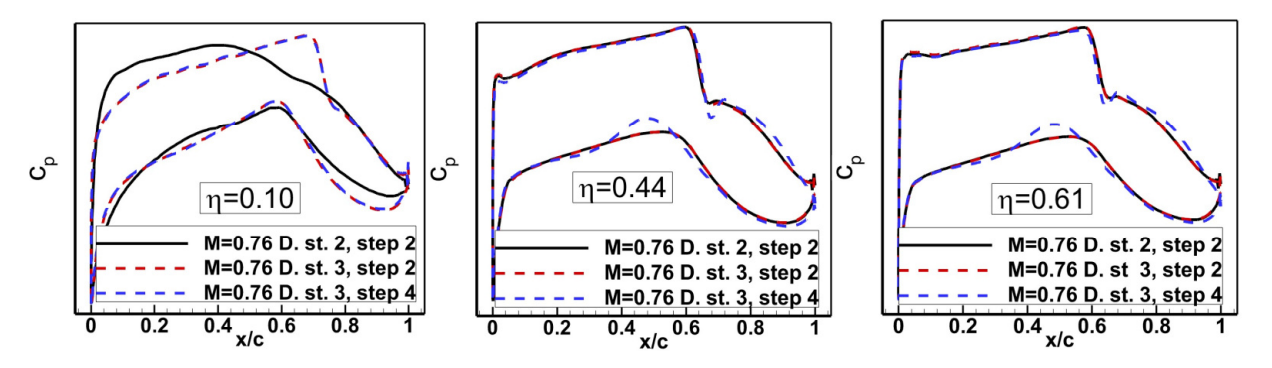


Figure 6: Case B, NLF wing design pressure distributions for η=0.10, 0.41 and 0.61.

4.3 Detailed NLF shape design for case B, M_∞=0.76, Δ_{ΦLE}=2.5°

For case B two initial wing body geometries were provided by Airbus denoted Design status 2 and 3. Additionally, a fuselage with slightly adapted belly fairing was provided. Initial wing twist was provided for the required circulation distribution for the case with turbulent boundary layer. The corresponding NLF wing was obtained, applying the detailed design procedure described in section 4.1. This procedure was applied for Design status 2 up to step 2 and for Design status 3 up to step 4. Figure 6 shows pressure distributions results for the detailed design. The shown results are for design procedure performed up to step 2 for Design status 2 (black) and Design status 3 (red) and Design status 3, step 4 (blue). Design status 2 and 3 differ in the inner wing and for a region in the tip region. Regarding transition due to Tollmien-Schlichting instability at the upper side at the innermost wing region, Design status 3 has a pressure distribution characteristic which is more favorable for laminar design. Also, the shock position is further downstream, see section η =0.10 in Figure 6. Inner wing differences between Design status 2. and Design status 3 extend up to η =0.40. As shown in Figure 7. Design status 3 shows an improved transition position in comparison to Design status 2. However, for a larger part of the inner wing transition occurs close to the leading-edge. The reason for this is, that the larger LE sweep of case B leads to transition in the nose region due to crossflow instability.

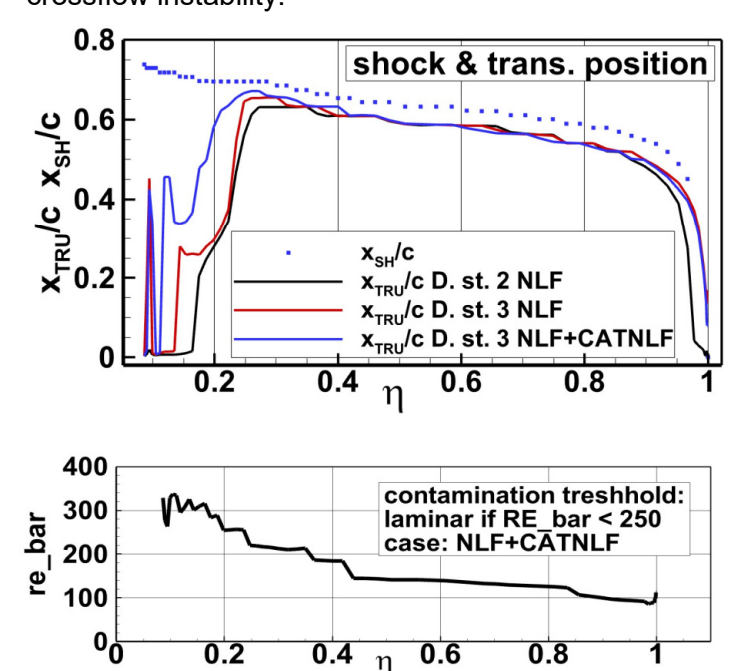


Figure 7: NLF design for case B. Upper wing: Relative transition and shock position (upper side) Spanwise distribution for attachment line criteria (lower side).

design will be denoted Case B NLF design.

Therefore, for improving the laminar extent, CATNLF design was required for the inner wing. Before considering the 3D design, it was useful to perform a 2.75D design for an inner section at η =0.20, which is described in the next section. Figure 7 shows that for a small region located close to the root section a large laminar extent is obtained. reason for this is that the 3D flow in the root region leads to an effective LE which is significantly sweep [15] reduced in comparison geometrical LE sweep. However, in reality at the LE of the root section a turbulent wedge will occur. Therefore, in the design process, laminar flow will not be considered for a spanwise region (about 3% span) close the root section. Besides the wing design described in this section for case B also the belly fairing was modified with the aim to reduce flow separation tendency at the trailing edge in the root region [24]. In the following the Design status 3 step 4

4.3.1 2.75D CATNLF design for inner wing section

Crossflow instability at the nose is very sensitive to the LE sweep. To avoid early transition due to crossflow instability CATNLF design [7]-[9] is used. At the nose the pressure distribution has a large

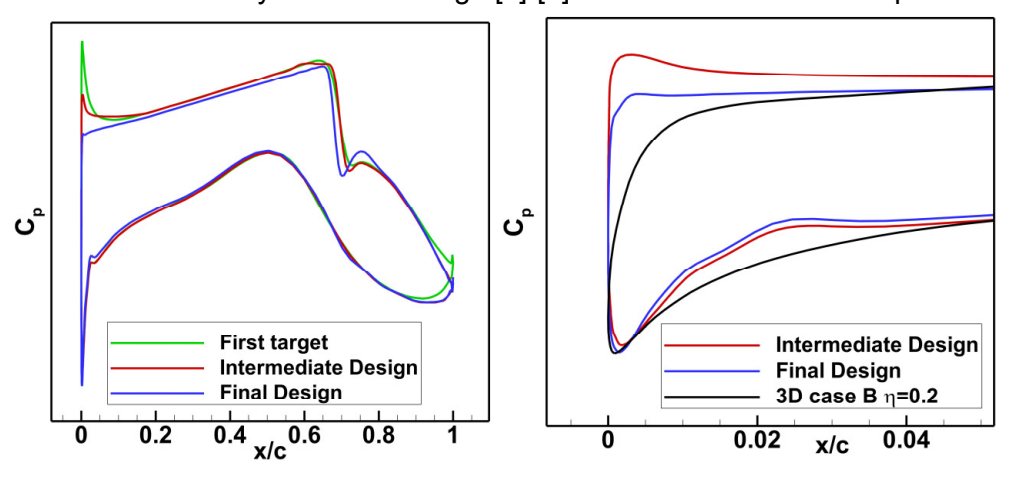


Figure 9: Case B, 2.75D design for η =0.20. Upper side complete pressure distribution, Lower side nose region.

gradient pressure which for traditionally designed NLF airfoils increases crossflow instability. **CATNLF** designed pressure distributions the pressure gradient is very steep at the nose followed by a pressure distribution which has very small gradient. To avoid transition at the side upper the pressure gradient in the nose region has

to be steep enough so that the almost constant pressure level of the upper side is reached before N_{CF} begins to grow. Here 2.75D design is used to obtain a target pressure distribution for the inner wing sections which gives the required nose pressure distribution to avoid crossflow transition for the LE sweep of case B. For 2.75D design the section η =0.20, was selected. Flow conditions correspond to the local flow condition of this section. Using 2.75D inverse design a geometry was designed using a first target pressure distribution with following properties: a) Except for the nose the local η =0.20 pressure distribution of the case B NLF solution for Design status 3 is used as target. b) The target pressure distribution has a steeper gradient in the nose region and corresponds to the 2.75D analysis of a previously DLR CATNLF airfoil [9], denoted airfoil A, which was designed

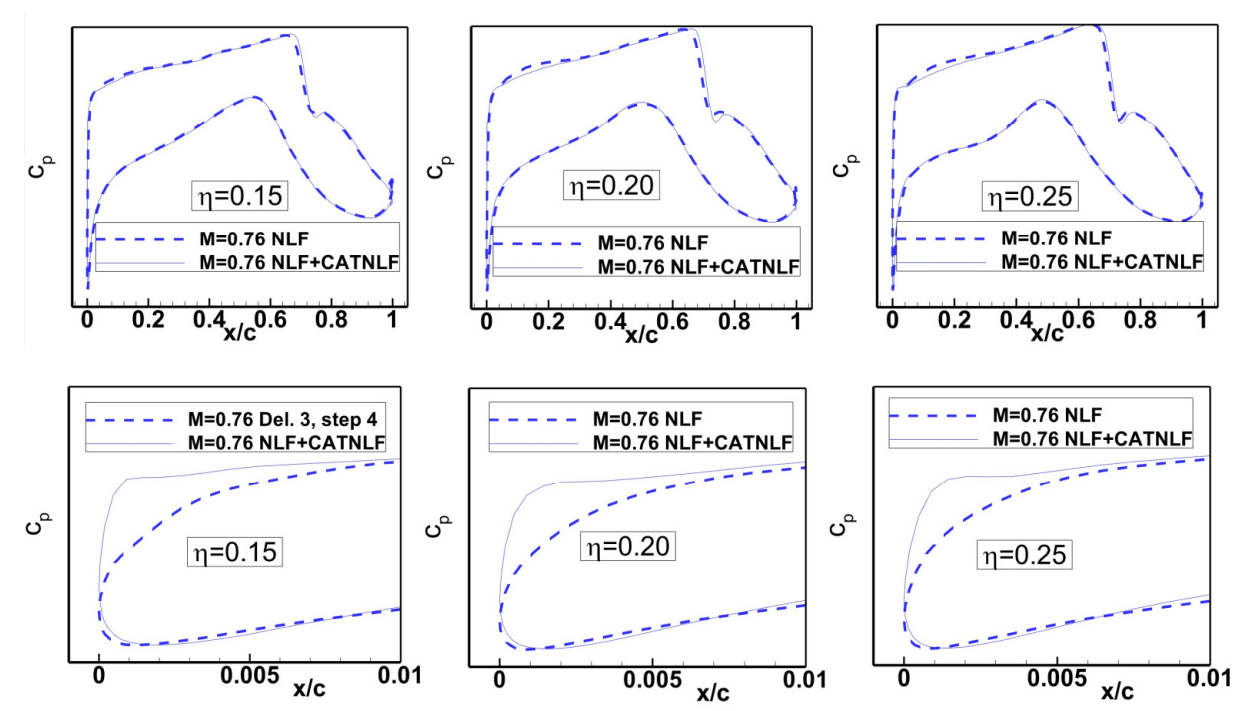


Figure 8: Case B, Inner wing design. Comparison between pressure distributions NLF design with NLF+CATNLF design. Upper row complete pressure distributions. Lower row restricted to nose region.

for another Mach number. Here analysis solution for airfoil A is obtained for η =0.20 case B local flow conditions. The so constructed first target pressure distribution is given in the left side of Figure 9. Starting geometry was airfoil A geometry. After adaptions of the target several inverse designs were performed, Figure 9, shows intermediate and final designed pressure distribution. The right side of Figure 9 compares these distributions in the nose region with the pressure distribution of the case B

wing section for η =0.20. Note how a much steeper gradient has been achieved.

4.3.2 3D inverse design (NLF +CATNLF)

In the next step, the final 2.75D CATNLF pressure distribution was used to construct the 3D CATNLF

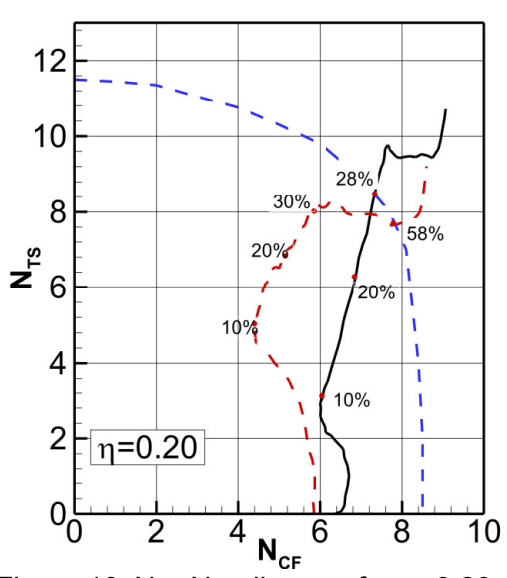


Figure 10 N_{CF} - N_{TS} diagram for η =0.20. Comparison between NLF design (black line) and NLF+CATNLF design (red line). Critical N-factors (blue line).

target pressure distribution for the inner wing design. For that purpose, the case B NLF pressure distributions were modified in the span region $\eta_{root} < \eta < 0.40$. Figure shows the comparison of the designed pressure distribution for the traditional NLF design with the NLF+CATNLF design. With increasing number of inverse design iterations, the nose gradient of the designed wing sections approached the 3D target pressure distribution. Here, the number of iterations was stopped after the designed pressure distribution gradient in the nose region was sufficiently steep so that transition due to crossflow was avoided. This was done in order to not comprise the low speed properties of the clean wing in addition. Figure 10 shows the N_{CF}-N_{TS} diagram for η =0.20. Note that the NLF+CATNLF design is more robust and the transition occurs at x/c=0.58, instead of x/c=0.28 for the NLF design. For the complete span distribution results for the NLF+CATNLF design transition position and for \overline{Re} are given in Figure 7. For the inner wing the region with laminar boundary has been increased. The free stream transition NLF design showed a reduction of drag in 8.6% of the total

drag $c_{D_{-}7g_{-}f.s}$ in comparison to the original Design status 3 configuration with turbulent boundary layer. With the NLF+CATNLF design this drag reduction was increased by further 0.7% of the total drag $c_{D_{-}7g_{-}f.s}$. For the inner wing for span less than η <0.20, values of \overline{Re} are greater than the laminar contamination threshold \overline{Re} =250, see Figure 7. Without contamination, the attachment line transition threshold is for \overline{Re} > 580.

4.4 Initial detailed NLF shape for case C, M_∞=0.77, Δφ_{LE}=5.0°

For the wings considered in the NLF BSW design exploratory study, case C has the largest cruise Mach number with M_{∞} =0.77. It is designed for a wing with the maximum LE sweep increase of $\Delta\phi_{\text{LE}}$ =5.0°. Two initial wing body geometries were provided by Airbus denoted Design status 4 and

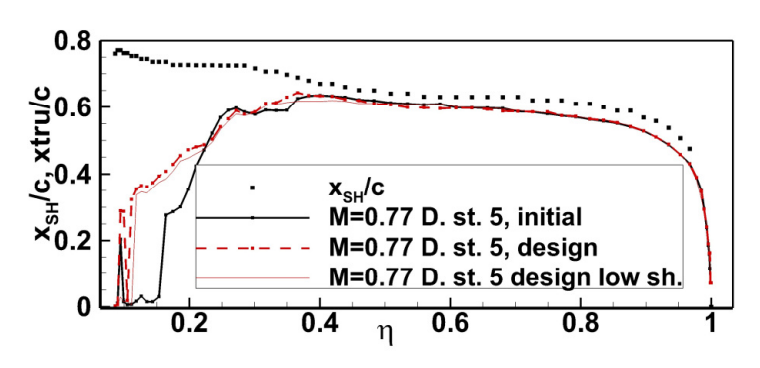


Figure 11: Design status 5. Upper wing: relative transition and shock position

5. Design status 5 differs from Design status 4 in the planform. Wing geometries were constructed using the airfoils of the design Mach=0.76 NLF+CATNLF described in section 4.3.2. For the M_∞=0.77 cruise design point Design status 4 and Design status 5 provide the distribution and thickness distributions which for NLF have to be satisfied as requirement. In contrast to previous deliveries the geometries of Design status 4 and 5 already have a twist distribution which satisfies the circulation distribution

requirement for the free transition case. Further design of case C is based on Design status 5. It is described in section 5.

5. Final ULTIMATE NLF wing design for M_∞=0.77, ΔφLE=5.0°

In this section the design of the final ULTIMATE BSW NLF wing for M_{∞} =0.77, Δ LE sweep $\Delta \varphi_{LE}$ =5° is described. In the previous study, the design was performed at the design cruise point. For off-design conditions evaluation occurred with the analysis of the designed cruise point geometry. To obtain the final ULTIMATE NLF wing, a design was performed at cruise design and off-design conditions with the aim to achieve a good compromise between large laminar extent and a good wave drag standard. Different design steps will be described in the next section. The aerodynamic evaluation of the final ULTIMATE NLF wing will also be presented.

5.1 3D inverse design (NLF+CATNLF) for Design status 5

For the initial Design status 5 geometry the inner wing transition occurs close to the LE, see Figure 11. This occurs, despite that the CATNLF airfoils designed previously for Ma_∞=0.76 were used in the Design status 5 initial NLF wing geometry. Therefore, due to the larger LE sweep of this case further CATNLF design was required. After several shape designs using the 3D inverse code, a larger region of laminar boundary layer was obtained for the inner wing, see Figure 11. In Figure 12 the pressure

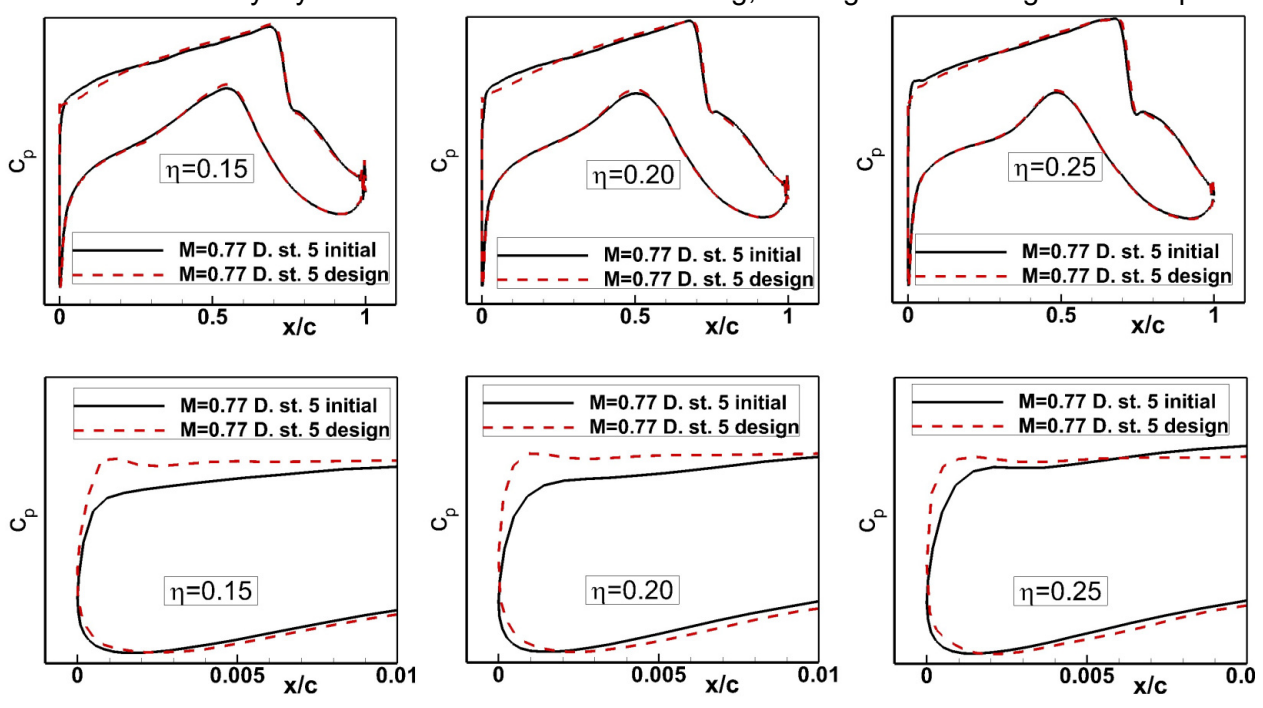


Figure 12: M_{∞} =0.77 wing Design status 5 inner wing design. Upper row; Complete pressure distributions. Lower row: C_p restricted to nose region.

distribution for inner wing sections of the initial and designed Design status 5 wings are compared. Note that in the nose region, 0 < x/c < 0.01 of the designed geometry a pressure gradient is obtained which has an initial steeper gradient and which is followed by an almost constant pressure distribution. On the upper side the pressure distribution in the region upstream of the shock was also

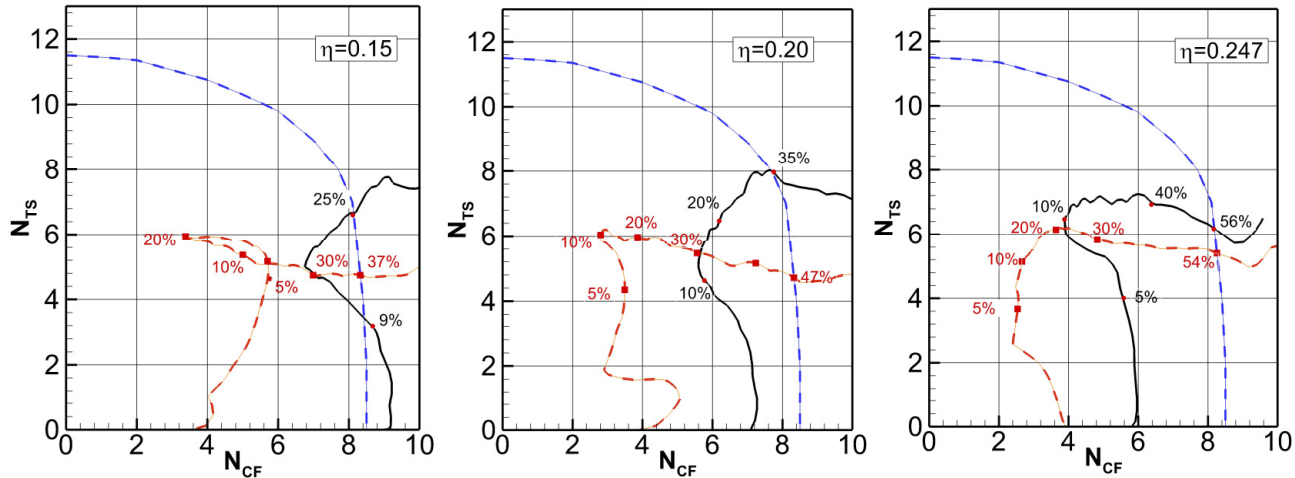


Figure 13 N_{CF} - N_{TS} diagram for Design status 5 wings. Initial wing (black line), designed wing (red line), critical N-factors (blue line). η =0.15 (left), η =0.20 (middle) and 0.247 (right).

11

changed. Smaller changes at the lower side are performed in order to satisfy the airfoil thickness requirement. After the inverse design steps, it was also necessary to slightly re-twist the wing in order to satisfy the load distribution.

Stability analysis results are given in Figure 13, which shows N_{CF} - N_{TS} diagrams for selected inner wing sections. Note that for the designed geometry not only transition was moved downstream, but also the N_{CF} - N_{TS} curves show a larger distance to the critical N-factor curve. Therefore, concerning transition also a more robust design was achieved. Within this work a special treatment of the stability analysis was required for N_{CF} , since the standard *lilo* [20] procedure did not find all amplified modes. This was especially the case for some wing sections with CATNLF design.

5.2 Further design steps

The analysis of the initial Design status 5 wing showed that high wave drag levels for $M_{\infty} \ge 0.77$ 1g lift conditions. The lower side of Figure 14 shows the spanwise wave drag for Design status 5 for the $M_{\infty} = 0.77$ cruise design point. Especially, the inner wing and the kink region contain large local wave drag. To decrease this drag component, drag planform modifications were performed as well as detailed wing shape modifications. The latter were performed at the $M_{\infty} = 0.77$ cruise design point and at higher off-design 1g cruise conditions. These modifications are described next.

5.2.1 Planform modifications: Wing geometries Design status 6 and 7

Two new planforms modifications were analyzed. The new wing geometries are denoted Design

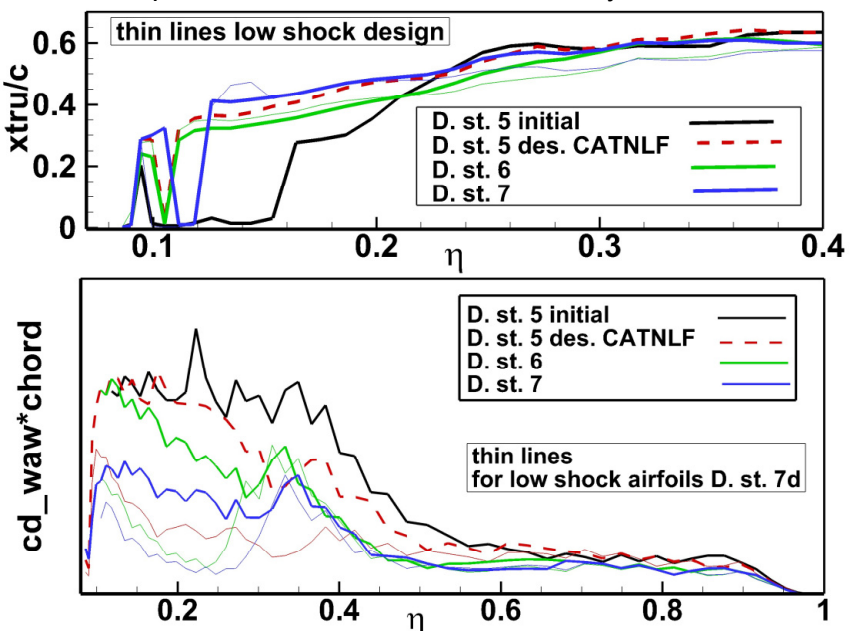


Figure 14 Spanwise transition and wave drag force for geometries: Design status 5 - Design status 7.

status 6 and Design status 7. geometries Both wing are constructed with the modified airfoil sections obtained in section 5.1. For the new planforms the LE sweep is not altered. To reduce the local c_i in the inner wing and kink section region in comparison to Design status 5 following modifications done: The kink section chord length for Design status 6 was increased and both the kink and root section chord lengths were increased for Design status 7. As a result, in comparison to Design status 5 wing area was increased by 1.9% for Design status 6, 2.4% for Design status 7. Results for the transition and wave drag distribution are given in Figure 14. Note that wave drag has been

reduced with the new planforms. In comparison to Design status 5, Design status 6 reduced the wave drag by 1.5% of the total drag $c_{D_{-}7g_{-}f.s.}$, whereas Design status 7 reduced the wave drag by 1.9% of the total drag $c_{D_{-}7g_{-}f.s.}$. Since Design status 7 shows less wave drag and has a better transition position, further studies were based on this geometry.

5.2.2 Wave drag reduction, inverse design for cruise design and off-design conditions

To reduce the wave drag of the ULTIMATE BSW, detailed shape designs were performed for the cruise design point and at off-design flow conditions. Simultaneously to the planform study described in section 5.2.1, a shape design to reduce wave drag was already performed for the CATNLF design of Design status 5. This was done at the 1g cruise design point. Figure 15 shows a comparison of pressure distributions for target, initial and designed geometry after 9 3D inverse design iterations. This shape modification was effective to reduce the wave drag in the inner wing and kink region, i.e. reducing it from 4.3% to 2.1% of the total drag $c_{D_{-}7g_{-}f.s.}$ As shown in Figure 11 the transition position for this low shock design shows only small changes to the Design status 5 CATNLF design. Using

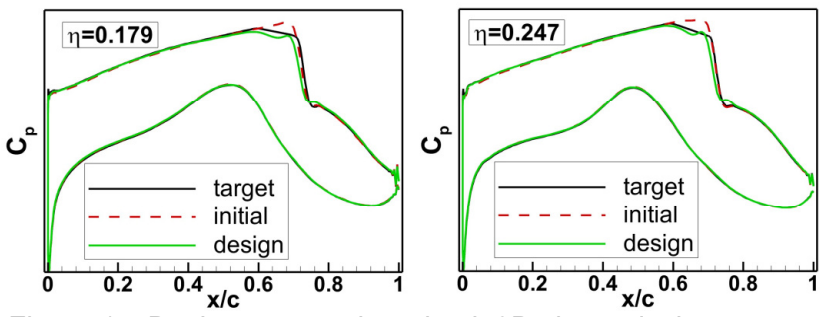


Figure 15 Design status 5 low shock 3D shape design

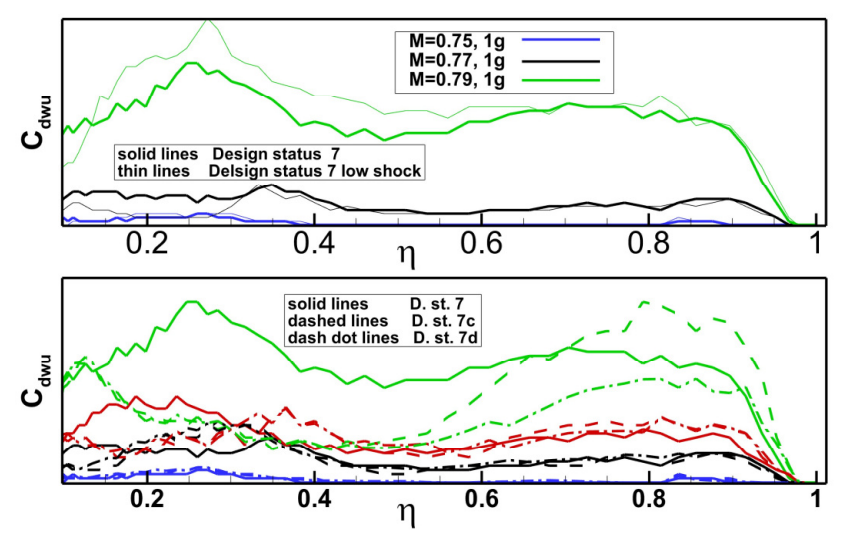


Figure 16 Local wave drag, Design status 7, 7 low shock, 7c and 7d. M_{∞} =0.75, 1g (blue lines), M_{∞} =0.77, 1g (black lines), M_{∞} =0.78, 1g (red lines) and M_{∞} =0.79, 1g (green lines).

these newly designed airfoils to construct the wing for the Design status 7 planform reduced the wave drag further from 2.4% to 1.5% of the total drag $c_{D 7g f.s}$ at the design point. Nevertheless, as shown in Figure 16 an offdesign study indicated that wave drag for higher Mach numbers. i.e. especially $M_{\infty} = 0.78$ and 0.79, was still rather high. Therefore, additional inner wing and kink region shape design performed for the M_∞=0.78 and the M_∞=0.79 1g flow conditions. The resulting geometry of these designs is denoted Design status 7c. These designs reduced the total wave drag in both spanwise regions at M_∞=0.78 and M_∞ =0.79. But at M_∞=0.79 for the region n> 0.5 the local wave drag increased to a level larger than Design status 7, see Figure 16, lower row. Due to the small chord length of the outer wing, the relative contribution of this region to the total wave drag is small, but the associated strong shocks are not desirable. Therefore, in the next step an outer wing

shape design was performed at the M_∞ =0.79 1g flow condition. The resulting geometry for this inverse design is denoted Design status 7d. As indicated in the lower row of Figure 16 for the Design status 7d geometry the level of wave drag in the outer wing was reduced. Table 2 summarizes the total wave drag values for the different shape designs. Note that for Design status 7d at M_∞ =0.77 the wave drag was increased in comparison to the Design status 7 low shock geometry (see Table 2), however for the higher Mach number M_∞ =0.79 there is a large decrease of wave drag in comparison to Design status 7. Despite the reduced shock strength in the outer there is incipient separation behind the shock for M_∞ =0.79, 1g flow condition due to the high level of local c_1 values.

Table 2: Wave drag⁺ comparison for different design status at different Mach numbers

Mach	Design status 5 CATNLF %	Design status 5 low sh. %	Design status 7 %	Design status 7 low sh.*	Design. status 7c**	Design status 7d*** %
0.75			0.2		0.4	0.4
0.77	4.3	2.1	2.4	1.5	2.4	2.1
0.78			4.5		3.9	3.9
0.79			> 12.9		7.5	6.4

⁺ all wave drag values related to c_{D 7g f.s.}, the total drag of free transition total drag design status 7g

Besides the inverse design geometry modifications, all wing results presented in this section included

^{*} Design status 7 low shock = design inner wing M_∞=0.77

^{**} Design status 7c=design inner wing Ma_∞= 0.78 and 0.79, correct twist and t/c

^{***}Design status 7d= design outer wing Ma_w=0.79, correct twist and t/c

minor modification to find: a) the twist distribution which satisfies the load distribution and b) to adjust the airfoils thickness to the target.

5.3 Analysis: TAU-RANS solutions on the fine analysis mesh

Most of the results presented previously were obtained using CFD-FLOWer solutions on the structured meshes. Here TAU CFD results are presented for the fine analysis mesh for 1g cruise flow conditions and for off-design. Results are presented for geometries Design status 7f and Design status 7g. Design status 7f and 7g resulted from Design status 7d through geometry smoothing operations to allow a better manufacture of the ULTIMATE BSW. Also, minor geometry deficiencies were corrected for example in the TE region without deteriorating the aerodynamic performance. For the root section flow separation tendency in the TE region was diminished.

5.3.1 Design status 7f, drag breakdown for design cruise point

Drag breakdown for Design status 7f is given in *Figure 17* for the free transition case. Values are given for the friction drag C_{Df} , the viscous pressure drag C_{Dpvi} , the wave drag C_{Dwav} and the induced drag C_{Dind} . The drag components are related to the total drag. Note that the large aspect ratio of the ULTIMATE BSW results in a lower induced drag contribution. In comparison to the DLR JTI BSW configuration [5], the ULTIMATE BSW configuration has a larger part of friction drag which is attributed to the longer fuselage.

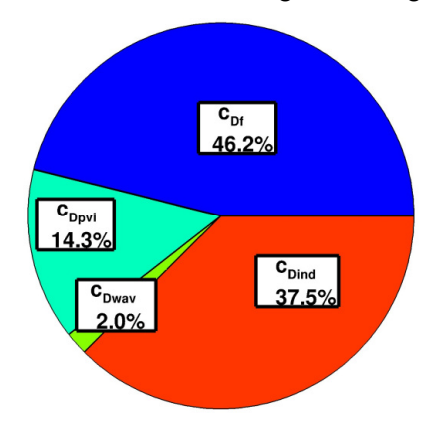


Table 3 Design status 7g: Performance cruise design point

Boundary Layer	Mesh	(L/D) _{rel} *	(Ma·L/D) _{rel} **
turbulent	DLR	1.123	1.109
free transition	DLR	1.249	1.233
turbulent	Airbus	1.141	1.126
free transition	Airbus	1.272	1.256

Figure 17 Design status 7f: Drag breakdown for cruise design point

5.3.2 Design status 7g, pressure distributions and transition position

Pressure distributions are shown in Figure 19 upper row for a lift sweep at M_{∞} =0.77 and in the lower row for a Mach sweep at 1g lift condition. To consider the properties of the clean wing, solutions at off-design were also obtained at a low Mach number M_{∞} =0.60. For this case transition occurs at the nose, (results not shown here). Transition position for a C_L sweep is shown for different Mach numbers in *Figure 18*. Solutions were obtained using the SOLAR meshes. For the transonic cruise with Mach and lift in the range $0.75 < M_{\infty} \le 0.78$, $0.95 \le C_L/C_{L_1g}(M_{\infty}) \le 1.05$ a robust transition is obtained. At M_{∞} =0.75 for the higher lift values transition moves to the nose. This is caused due to a nose suction peak. Additional work to increase the laminar extent at M_{∞} =0.75 will be presented in section 5.4. Lower left side of *Figure 18* shows results for the attachment line criteria \overline{Re} . The values are less than the upper threshold \overline{Re} =580 for attachment line transition and most of the wing has \overline{Re} values <250, which is the \overline{Re} transition threshold for which flow remains laminar despite contamination.

^{*(}L/D)rel=(L/D)/ (L/D)ref , **(Ma·L/D)rel=(Ma·L/D)/ (Ma·L/D)ref

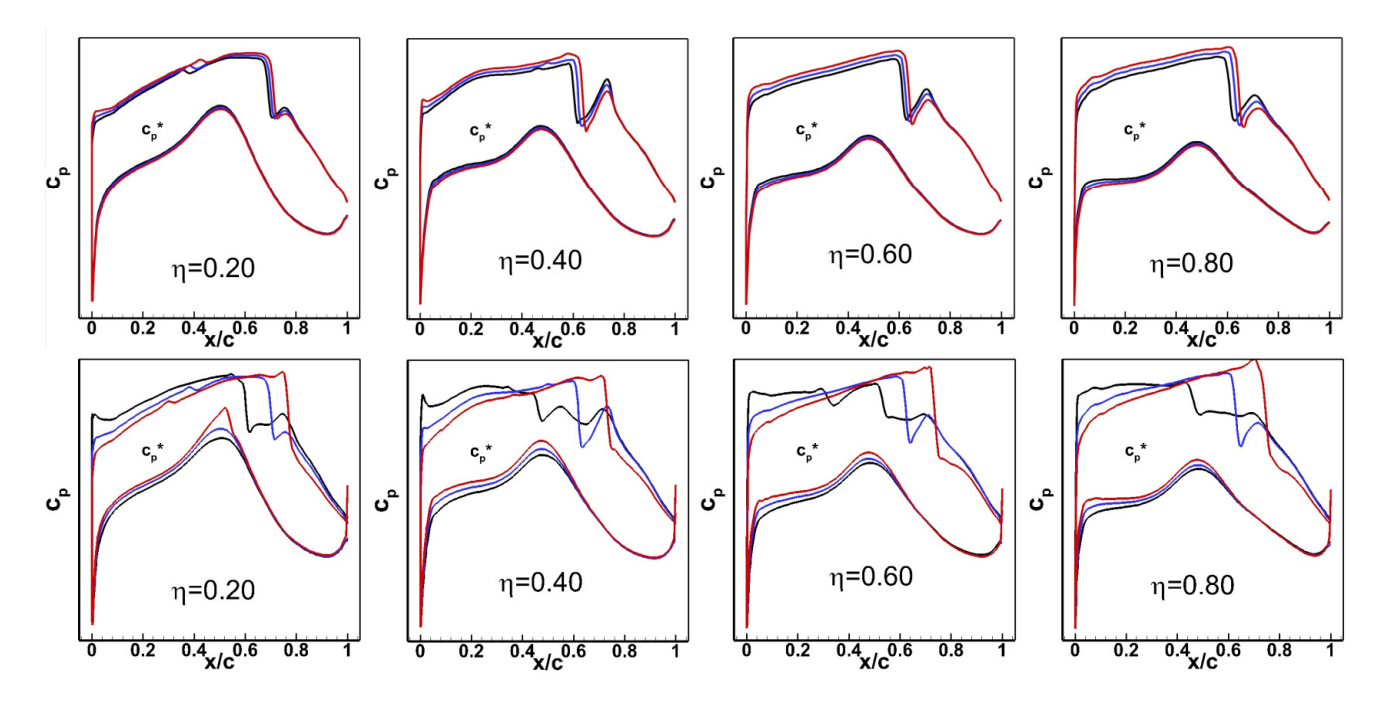


Figure 19 Design status 7f: Pressure distributions. Upper row for C_L sweep for design Mach cruise number M_{∞} =0.77. C_L =0.95g (black line), C_L =1.00g (blue line) and C_L =1.05g (red line). Lower row for Mach sweep for 1g C_L flow conditions. M_{∞} =0.75 (black line), M_{∞} =0.77 (blue line), M_{∞} =0.79 (red line).

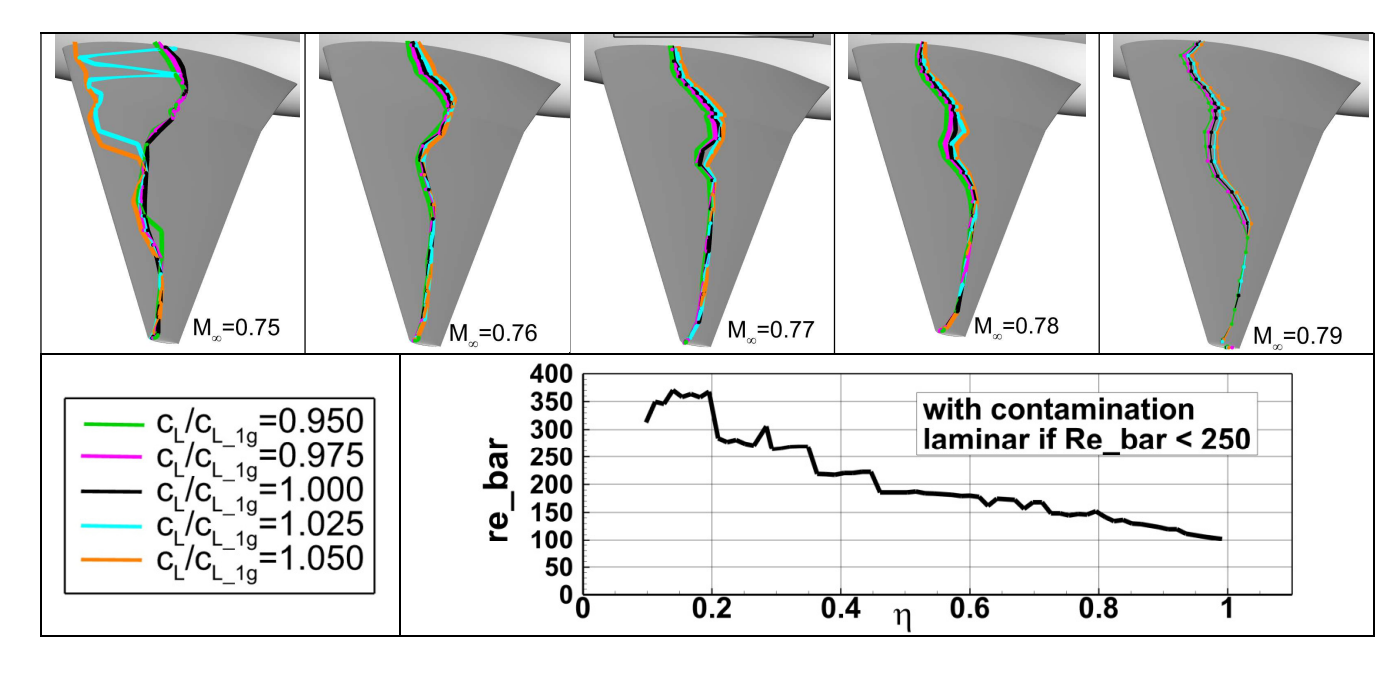


Figure 18 Design status 7f: Transition positions for a lift sweep for different Mach numbers. From left to right M_{∞} = 0.75, 0.76, 0.77, 0.78 and 0.79. Lower left side: spanwise distribution for attachment line criteria \overline{Re} for cruise design point.

5.3.3 Performance: L/D and aerodynamic efficiency

At the M_∞=0.77 cruise design point for Design status 7g both the SOLAR mesh results and the Airbus meshes result in an aerodynamic efficiency improvement of 23.3%/25.6% and a L/D improvement of 24.9%/27.2%, see Table 3. Values of L/D and aerodynamic efficiency are normalized with corresponding reference values for a generic middle range aircraft. These reference values correspond to the cruise design point for a wing-body configuration designed for turbulent boundary

layer. In comparison to this reference aircraft the ULTIMATE NLF BSW wing-body configuration shows a substantial improvement. This is due to: a) the reduction of induced drag, what is attributed to the large aspect wing ratio and b) the reduction of viscous drag which is attributed to the large laminar boundary layer extent. The ULTIMATE NLF BSW also shows an improvement in comparison to the DLR JTI NLF/LFC BSW design [5], for which in comparison to the turbulent reference wing-body geometry a significant performance increase was achieved. Note also that the DLR JTI NLF/LFC BSW design was designed with a laminar boundary layer for upper and lower wing side and for the inner wing a laminar boundary layer was obtained with an LFC design. Using the SOLAR mesh, CFD solutions for the Design status 7g configuration were obtained for a complete field including off-design flow conditions with: $0.75 \le M_{\odot} \le 0.79$ and $0.95 \le C_L/C_{L_1g}(M_{\odot}) \le 1.2$. For this field, contour plots are shown in Figure 20 for the L/D ratio and the aerodynamic efficiency $M_{\odot} \cdot L/D$. In the plots C_L is normalized with the Mach M_{\odot} =0.77 1g C_L value, denoted $C_L(1g_077)$. The relative maximum aerodynamic efficiency value obtained is 1.272. This is not achieved for the cruise design point, but for a lift corresponding to 1.1g. Note that the aerodynamic performance improvement is larger than 1, also for the entire range of off-design conditions shown in Figure 20.

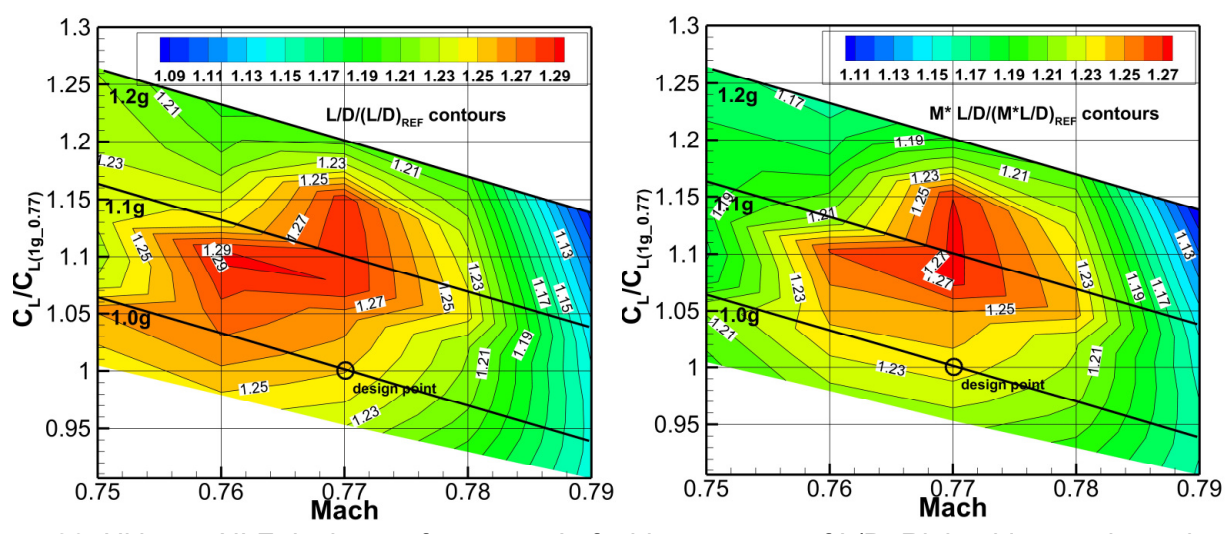


Figure 20 Ultimate NLF design performance. Left side: contours of L/D. Right side aerodynamic performance.

5.4 Improvement of laminar extent for lower Mach numbers using variable camber flaps

Previous work has shown that variable camber flaps can improve the laminar performance at off-design significantly when considering an isolated airfoil [3]. Therefore, it was decided to apply a similar procedure to the final ULTIMATE BSW geometry in order to assess what kind of improvements could be expected for a 3D geometry. The chosen camber flaps had a chord length of 0.15 x/c and deflections of δ =0°, 1° and 2° were considered. The work was focused in the off-design case at Mach M_{∞} =0.75, where the CATNLF suction peak leads to early transition and reduced laminar flow due to the increased angle of attack.

In *Figure 21* results for the transition position and pressure distributions of selected sections are given at M_{∞} =0.75. The left side shows results for C_L corresponding to 1g, the right side for C_L corresponding 1.025g. The results showed that a 1° deflection leaded to an angle of attack reduction of 0.4° and drag reduction of 0.8% of the total drag $c_{D_{-}7g_{-}f.s}$ for 1g case at the M_{∞} =0.75. For the corresponding 1.025g case, the same deflection leaded to an angle of attack reduction of 0.7° and drag reduction of 3.4% of the total drag $c_{D_{-}7g_{-}f.s}$. Note how for the 1.025g case with δ =1° the transition line is moved from the nose region to a position similar to the one obtained for the 1g case with δ =1°. For the M_{∞} =0.75, 1g case, a deflection of 2° was also investigated, and although the angle of attack was further reduced, no drag reduction was encountered compared to the 1° deflection. A drag breakdown showed, that the friction drag was reduced from 0° to 1° and stayed constant for a further deflection increase from 1° to 2°. Furthermore, it showed that the wave drag increased by 1.3% of the total drag $c_{D_{-}7g_{-}f.s.}$

Additionally, as shown in Figure 21 left side, it was observed that despite the camber flap improved the overall performance, the laminar extent was reduced at the inner wing with increasing camber

flap deflections. Further investigation showed that the gradient was already high enough in this region without camber flap deflection, a stronger acceleration due to the camber flap only caused earlier CF transition. Therefore, one could expect further improvements through the implementation of a camber flap already from the beginning.

The study has shown that a camber flap has a huge potential in order to improve performance of cruise off-design conditions. Further work and detailed design are needed for optimizing the overall performance.

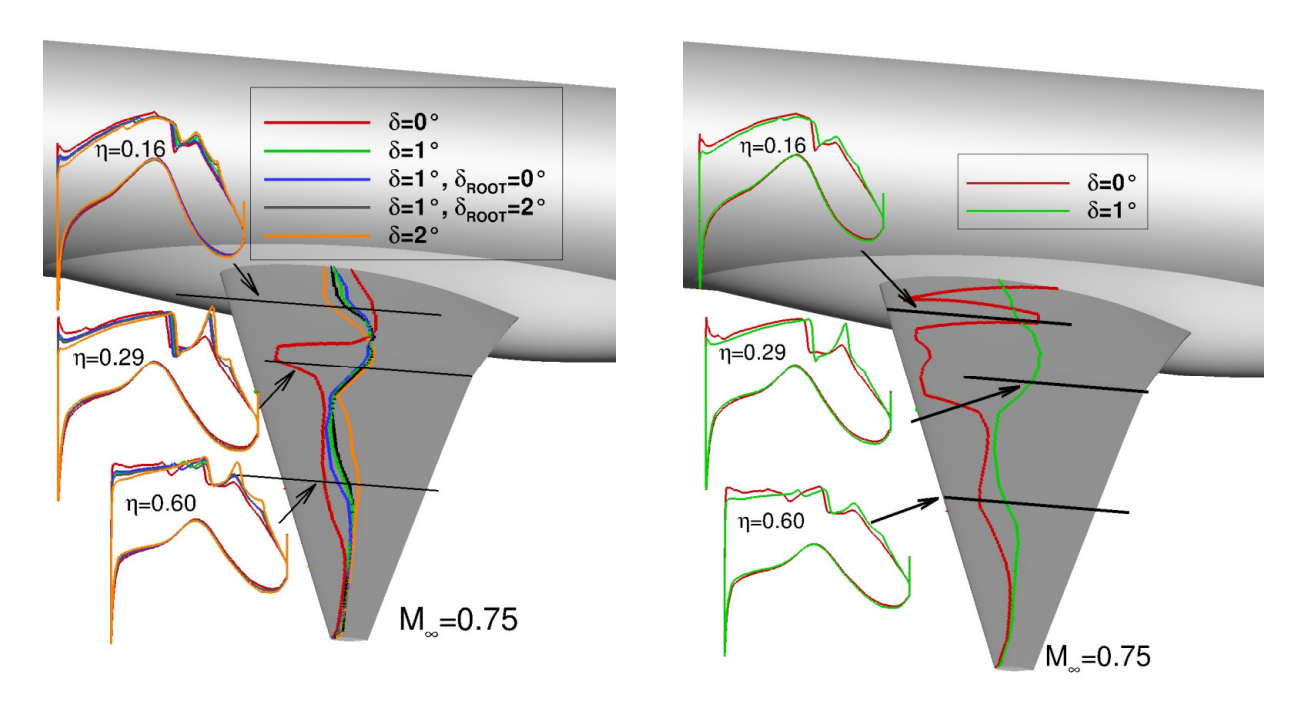


Figure 21 Camber Flap: M_{∞} = 0.75, pressure distributions and transition positions C_L/C_{L_1g} =1 (left side) and C_L/C_{L_1g} =1.025.

6. Wind tunnel model geometry smoothing and jig shape

The designed ULTIMATE BSW geometry provided the twist flight shape and the jig bending geometry. The construction of the wind tunnel model requires a smooth surface of the jig twist and bending shape. After the design considerable work is required to obtain this.

6.1 Geometry smoothing

As previously described, the 3D inverse design geometry is transferred from its 3D inverse design tool FLOWer solution to the 3D CAD software CATIA. This is done by means of a point-based airfoil format. Due to imprecision during the transfer or due to data interpolation afterwards the airfoil curves in CATIA can show curvature oscillations.

Another source of non-desired curvature oscillation along the wingspan is the twist distribution and the profile differences. If for example, two, very different airfoils are placed close together, the differences between the airfoils can lead to oscillations in the guide curves along the wingspan, which later on can be observed in the surface. This effect can also happen if the twist between too very close airfoils changes to drastically.

Aerodynamic goals and curvature oscillation sources are difficult to tackle at the same time, keeping the aerodynamic goals. A deep aerodynamic understanding is required in order to identify what is a feature and what is a non-desired curvature oscillation. Therefore, usually the aerodynamic goals are achieved first before the curvature oscillations are removed.

For the here presented geometry, much work was invested in geometry smoothing in order to achieve a high degree of surface standard that is necessary for a production aircraft.

6.2 Jig shape and CAD construction

The wind off shape is developed based on the aerodynamic loads and the structural model of the wind tunnel model construction. The target twist distribution has to be achieved at aero design point under corresponding wind tunnel conditions, i.e. pressure and temperature,

In the current case the wing bending is not handled as design target but as a deformation result, which may need some final adaptation to keep the target load distribution at design point.

The high aspect ratio of the wing affects the flexible behavior of the shape significantly, leading to more deformation than current single-aisle wing design. Therefore, the correct prediction of the resulting flight shape in the tunnel is mandatory to achieve the same aerodynamic performance in the experiment as predicted in the previous design study.

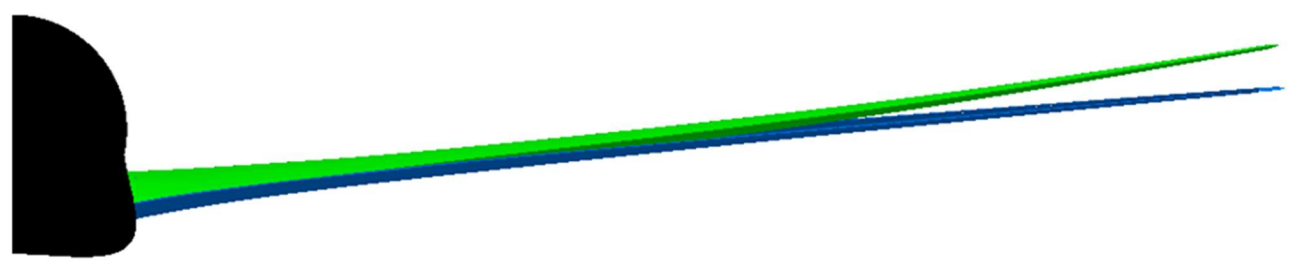


Figure 22 Comparison of jig (blue) and flight (green) wing shapes.

The final geometry smoothing has to be conducted on the wind off shape before model manufacturing.

7. Summary and outlook

Within the national German project ULTIMATE new NLF BSWs were designed. One of the aims of the exploration study was to identify how much the cruise Mach number relative to previous NLF BSW designs can be increased. Previous BSW NLF designs, for example the DLR-JTI design had a cruise design Mach number of M_∞=0.75. As a result of the increased Mach number BSWs with larger leading-edge sweep have to be considered in order to guarantee an acceptable wave drag standard. Another target of the present laminar boundary BSW designs was to achieve a laminar boundary layer for the entire wing span solely by NLF design without boundary layer suction. Particularly, for the inner wing with increasing leading-edge sweep there is a tendency to have early transition at the nose due to crossflow instability. Traditionally with boundary layer suction in the nose region, this transition can be avoided. Unlike this approach, in the current study, a crossflow attenuated NLF (CATNLF) design strategy was applied in the leading-edge of the inner wing to avoid this transition. A third aim of this work is to provide for the final ULTIMATE NLF BSW design a wind tunnel geometry to conduct a test in the European Transonic Wind Tunnel (ETW) for performance and tool validation purposes.

In the present work wing body configurations were considered. In contrast to previous NLF BSW designs, in the present work large aspect ratio wings are considered. Therefore, the considered configuration will have reduced induced drag. In addition, the fuselage corresponds to a long single aisle configuration. Both the large aspect ratio and the large fuselage lead to large local lift values for the 1g condition. Due to the large lift values, a more careful design is needed to keep wave drag at acceptable level.

In this work, BSW NLF designs for free stream transition conditions were obtained which satisfy the previously mentioned targets, starting with design cruise M_{\odot} =0.75. In the following study Mach number was increased in steps of ΔM_{\odot} =0.01 and the wing leading-edge sweep was increased correspondingly in steps of $\Delta \varphi_{LE}$ =2.5°. The initial leading-edge sweep corresponds to the NLF panel of the BLADE NLF flight experiment. The final ULTIMATE NLF BSW design had a cruise Mach number M_{\odot} =0.77 with a wing that had a larger leading-edge sweep than the initial wing by 5°. Design procedure and results for both the initial M_{\odot} =0.75 and the intermediate M_{\odot} =0.76 ULTIMATE NLF BSWs are provided in this work.

For the final M_∞=0.77 ULTIMATE NLF BSW a more detailed wing design was performed which did not consider only the design cruise point but also off-design points. The results show a significant performance improvement. For the design cruise point, using CFD solutions obtained with differently generated meshes, on the average an aerodynamic efficiency improvement of 24.5% and a L/D

improvement of 26.5% is obtained. This compares with a previous DLR BSW design, the DLR-JTI design, for which a significant improvement of aerodynamic efficiency was achieved. The relative values are related to a reference value for a generic middle range aircraft which correspond to the cruise design point for a wing-body configuration designed for turbulent boundary layer. The improvement of performance extends to a large cruise off-design region considered in this work. It is due to reduction of induced drag and viscous drag. The reason for the former drag component reduction is the large wing aspect ratio while viscous drag was decreased due to the laminar boundary layer. For the off-design conditions considered, except for M_{∞} =0.75 the final ULTIMATE NLF BSW configuration shows a robust transition position which shows little deviations for different lift values for the considered Mach numbers. For M_{∞} =0.75, where for larger lift values transition was close to the nose, a larger extent of laminar boundary layer for the inner is achieved by using a variable camber flap.

The final ULTIMATE NLF BSW design provided the flight twist and jig bending geometry for the wind tunnel test for the design cruise point. The high aspect ratio of the wing affects the flexible behavior of the shape significantly, leading to more deformation than current SA wing design. The corresponding jig twist and flight bending geometry for the wind tunnel geometry were obtained. In addition, the final ULTIMATE NLF BSW wind tunnel geometry underwent a series of smoothing steps in order to achieve a high degree of surface standard that would be necessary for the manufacture of metallic production aircraft.

For the ETW test, future work will consider CFD solutions for the wind tunnel model at the ETW flow conditions. It would be interesting to perform a similar study as was done here for a BSW configuration also for an FSW. Due to the aerodynamic advantages which an FSW offers for laminar flow, current design of the DLR-FSW configuration had a design cruise point of M_{∞} =0.78. With CATNLF design strategy wings with larger leading-edge sweep could be also considered for an FSW, so that there is potential to also increase the design cruise Mach number of an FSW. For such a study, large aspect wings as the ones considered here should be considered, thus allowing additional performance improvement through reduction of induced drag.

8. Acknowledgement

The national project ULTIMATE is funded by German Federal Ministry for Economic Affairs and Energy within the German Aeronautical Research Program LuFo VI-2/2022- 2025 under grant agreement no 20A2101A. The authors want to thank Normann Krimmelbein for the large support provided in this work with the automatic transition determination which allowed the transition prediction with CATNLF wing sections.

9. Contact Author Email Address

mailto: th.streit@dlr.de

10. Copyright Statement

The authors confirm that they, and/or their company or organization, hold copyright on all of the original material included in this paper. The authors also confirm that they have obtained permission, from the copyright holder of any third party material included in this paper, to publish it as part of their paper. The authors confirm that they give permission, or have obtained permission from the copyright holder of this paper, for the publication and distribution of this paper as part of the ICAS proceedings or as individual off-prints from the proceedings.

References

- [1] <u>Gibson, T., Souchealeau, B., Rogers, N., "BLADE Natural Laminar Flow Testing, 32nd ICAS conference, Shanghai, China, September</u>
- [2] Larsson, R., "Analysis of the effect of Flow Transition over the Wings of the BLADE Demonstrator", 33rd ICAS conference, Stockholm, Sweden, September 2022.
- [3] Arne Seitz, A Hübner, and Kristof Risse. The DLR "TuLam project: design of a short and medium range transport aircraft with forward swept NLF wing", CEAS Aeronautical Journal, 11(2):449–459, 2020.
- [4] Ruberte Bailo, J., Seitz, A., Streit, T, "Belly-Fairing Design Space Exploration for a Forward Swept Natural Laminar Flow Aircraft", 57th International Conference on Applied Aerodynamics, Bordeaux, France, March 1923.

- [5] Streit, T., Wedler, S. and Kruse, M., "DLR natural and hybrid transonic laminar wing design incorporating new methodologies", Aeronautical J, 2015, **119**, (1221), pp 1303-1326.
- [6] D. Schwarmborn, T. Gerhold, R. Heinrich, "The DLR TAU-Code: Recent Applications in Research and Industry", *Proceedings of European Conference on Computational Fluid Dynamics ECCOMAS CFD 2006*, Delft, Netherlands.
- [7] Lynde, M. N. and Campbell, R., "Computational Design and Analysis of a Transonic Natural Laminar Flow Wing for a Wind Tunnel Model", AIAA 2017-3058, June 2017.
- [8] Campbell, R. L. and Lynde, M. N., "Natural Laminar Flow Design for Wings with Moderate Sweep", 34th AIAA Applied Aerodynamic Conference, AIAA AVIATION Forum, AIAA 2016-4326, June 2016., https://doi.org/10.2514/6.2016-4326.
- [9] Streit, T., Seitz, A., Hein, S., Kunze, P., "NLF Potential of Laminar Transonic Long-range Aircraft", AIAA Aviation 2020 Forum, 15-19. June 2020, USA Virtual Event, https://doi: 10.2514/6.2020-2748.
- [10] Schrauf, G., von Geyr, H., "Simplified Hybrid Laminar Flow Control for the A320 Fin Part 2: Evaluation with the e^N-method", AIAA-2021-1305, AIAA SciTech Forum, 11-15 & 19-21 January 2021.
- [11] Streit, T., Hoffrogge, C., DLR transonic inverse design code, extensions and modifications to increase versatility and robustness, *The Aeronautical Journal*, 2017, **121**, (1245), pp 1733-1757.
- [12] Kroll, N. and Fassbender, J.K. MEGAFLOW –Numerical Flow Simulation for Aircraft Design, *Notes on Numerical Fluid Mechanics and Multidisciplinary Design (NNFM)* vol. **89**, Springer Verlag, Closing Presentation DLR Project MEGAFLOW Braunschweig (de), 10–11 January 2002.
- [13] Seitz, A., Horstmann, K.H., Design studies on NLF and HLFC Applications at DLR, 27th International Congress on the Aeronautical Sciences, 19.-24. Sep., Nice, France, 2010.
- [14] Streit T., Kruse M., Kilian T., v. Geyr, J., Petropoulos I., "Aerodynamic Design and Analysis of HLFC Wings within the European Project HLFC-WIN", 33rd ICAS conference, Stockholm, Sweden, September 1922.
- [15] Streit, T., Wichmann, G., Campbell, R. L. and von Knoblauch zu Hatzbach, F., "Implications of conical flow for laminar wing design and analysis", AIAA Paper 2011-3808, 29th AIAA Applied Aerodynamics, Conference, 27-30 June 2011, Honolulu, HI, USA.
- [16] Wichmann, G. Untersuchung zur Flügel-Rumpf-Interferenz durch Anwendung eines Eulerverfahrens für kompressible Strömung, 1993, Dissertation, Institut für Strömungstechnik, Technische Universität Braunschweig, ZLR-Forschungsbericht 93-06.
- [17] Streit, Th., Wichmann, G. and Rohardt, C.-H. Nachrechnung und Entwurf von transsonischen Tragflügeln für die DO-728/DO-928, 1999, Technical Report, DLR IB 129-99/13, Braunschweig, Germany.
- [18] SOLAR 15.3.7 M Leatham, S Stokes, J A Shaw, J Cooper, J Appa, T A Blayloc. Automatic Mesh Generation for Rapid-Response Navier-Stokes Calculations, AIAA Paper 2000-2247, 2000.
- [19] Krimmelbein, N. and Krumbein A., "Automatic Transition Prediction for Three-Dimensional Configurations with Focus on Industrial Application", AIAA 2010-4292, 40th Fluid Dynamics Conference and Exhibit, Chicago, Illinois. https://doi.org/10.2514/6.2010-4292
- [20] Schrauf, G., LILO 2.1 Users Guide and Tutorial, GSSC Technical Report, July 2006.
- [21] Schrauf, G., COCO A Program to Compute Velocity and Temperature Profiles for Local and Nonlocal Stability Analysis of Compressible, Conical Boundary Layers with Suction, ZARM Technik Report, November 1998.
- [22] Van Der Vooren, J., and Destarac, D., "Drag/thrust analysis of jet-propelled transonic transport aircraft; definition of physical drag components," *Aerospace Science and Technology*, Vol. 8, No. 6, 2004, pp. 545–556
- [23] Destarac, D., "Far-Field / Near-Field Drag Balance and Applications of Drag Extraction in CFD, In: CFD-based Aircraft Drag Prediction and Reduction", VKI Lecture Series 2003, Von Karman Institute for Fluid Dynamics, Rhode Saint Genèse, February 3-7, 2003, National Institute of Aerospace, Hampton (VA), November 3-7,
- [24] Gruner, T., Aerodynamischer Entwurf einer Flügel-Rumpf-Verkleidung zur Integration eines laminaren Tragflügels, Bachelor Thesis TU-Braunschweig, 2022.0